THE JOURNAL OF BIOLOGICAL CHEMISTRY VOL. 290, NO. 49, pp. 29259–29269, December 4, 2015

The Cysteine-rich Domain of the DHHC3 Palmitoyltransferase Is Palmitoylated and Contains Tightly Bound Zinc*

Received for publication, September 7, 2015, and in revised form, October 19, 2015 Published, JBC Papers in Press, October 20, 2015, DOI 10.1074/jbc.M115.691147

Colin D. Gottlieb[‡], **Sheng Zhang**[§], **and Maurine E. Linder**[‡1]

From the [‡]*Department of Molecular Medicine and the* [§]*Core Proteomics and Mass Spectrometry Facility, Cornell University, Ithaca, New York 14853*

DHHC palmitoyltransferases catalyze the addition of the fatty acid palmitate to proteins on the cytoplasmic leaflet of cell membranes. There are 23 members of the highly diverse mammalian DHHC protein family, all of which contain a conserved catalytic domain called the cysteine-rich domain (CRD). DHHC proteins transfer palmitate via a two-step catalytic mechanism in which the enzyme first modifies itself with palmitate in a process termed autoacylation. The enzyme then transfers palmitate from itself onto substrate proteins. The number and location of palmitoylated cysteines in the autoacylated intermediate is unknown. In this study, we present evidence using mass spectrometry that DHHC3 is palmitoylated at the cysteine in the DHHC motif. Mutation of highly conserved CRD cysteines outside the DHHC motif resulted in activity deficits and a structural perturbation revealed by limited proteolysis. Treatment of DHHC3 with chelating agents *in vitro* replicated both the specific structural perturbations and activity deficits observed in conserved cysteine mutants, suggesting metal ion-binding in the CRD. Using the fluorescent indicator mag-fura-2, the metal released from DHHC3 was identified as zinc. The stoichiometry of zinc binding was measured as 2 mol of zinc/mol of DHHC3 protein. Taken together, our data demonstrate that coordination of zinc ions by cysteine residues within the CRD is required for the structural integrity of DHHC proteins.

Palmitoylation describes the attachment of a 16-carbon fatty acid to cysteine residues in proteins through a reversible thioester bond. Screens of the palmitoyl proteome have identified hundreds of palmitoylated proteins (1–4), including many involved in the pathogenesis of human diseases. Palmitate serves as a membrane anchor for many cytoplasmic proteins and is also present on numerous integral membrane proteins. The functions of palmitoylation are diverse and include the regulation of protein trafficking, stability, and activity (5–7).

DHHC[2] proteins catalyze the addition of palmitate onto substrate proteins. These enzymes comprise a highly diverse family with 23 members in humans. The association of DHHC proteins with a variety of diseases, including cancer, Huntington disease, and X-linked intellectual disability, highlights the biomedical importance of this enzyme family (8–10). DHHC proteins contain at least four transmembrane domains and a highly conserved cysteine-rich domain (CRD) between transmembrane domains 2 and 3 on the cytoplasmic face of membranes. The signature feature of the CRD is a nearly invariant DHHC (Asp-His-His-Cys) motif. *In vitro*, mutation of the cysteine in the DHHC motif blocks both autoacylation and transfer activity of DHHC palmitoyltransferases (11). This evidence has led to the hypothesis that this cysteine is the site of autoacylation. However, there is no direct evidence that the cysteine of the DHHC motif is palmitoylated. In cells, DHHC proteins are palmitoylated at steady state, and mutation of the cysteine in the DHHC motif appears to abolish detectable incorporation of palmitate (12). Mass spectrometry profiling of palmitoylated proteins in cells has revealed palmitoylation at a conserved cluster of cysteine residues in the C-terminal region of a subset of DHHC proteins (13). However, not all DHHC proteins contain these cysteine residues, and other sites of palmitoylation might be present (14, 15).

The presence of a conserved pattern of cysteine and histidine residues in the CRD originally led to the classification of DHHC proteins as zinc finger proteins (16–18). Recently, a model of the yeast Swf1 DHHC-CRD based on the crystal structure of the ubiquitin-protein ligase Pirh2 suggested that the CRD is built around two CCHC zinc fingers (19). Mutation of the cysteine and histidine residues assigned to the CCHC zinc fingers resulted in loss of function of Swf1 *in vivo*, and sequence comparisons suggest that there is selective pressure to maintain the CCHC pattern. The model is supported by experimental evidence that an isolated Swf1 DHHC-CRD expressed in bacteria and then purified and refolded in the presence of zinc binds ~2 mol of zinc/mol of protein (19). However, metal ion binding of an active and intact DHHC protein has not been reported previously.

In this study, we performed a structure/function analysis of the seven conserved cysteine residues within the DHHC-CRD using murine DHHC3 as a model enzyme. The CRD of DHHC3 has the pattern of conserved cysteine and histidine residues characteristic of DHHC proteins (Fig. 1*A*). In prior work (20), we have shown that catalytic activity of the enzyme is dependent upon Cys-157, the cysteine of the DHHC motif. However, the role of the other conserved cysteine residues in the function of DHHC3 is unknown. The focus of the present study was to identify sites of palmitoylation and determine whether the

* The authors declare that they have no conflicts of interest with the contents of this article.

[1] To whom correspondence should be addressed: CVM Box 41, Cornell University, Ithaca, NY 14853. Fax: 607-253-3659; E-mail: mel237@cornell.edu.

[2] The abbreviations used are: DHHC, aspartate-histidine-histidine-cysteine; CRD, cysteine-rich domain; CCHC, cysteine-cysteine-histidine-cysteine; FA, formic acid; HA, hydroxylamine; DDM, *n*-dodecyl-β-D-maltoside; Ni-NTA, nickel-nitrilotriacetic acid; PAT, protein acyltransferase; TCEP, tris(2-carboxyethyl) phosphine; biotin-HPDP, *N*-[6-(biotinamido)hexyl]-3′-(2′-pyridyldithio)propionamide; ACN, acetonitrile; ABE, acyl-biotin exchange; FT, Fourier transform; SEC, size exclusion column.

DHHC-CRD in an intact and active enzyme contains bound metal ions. We devised a mass spectrometry protocol that enables direct detection of palmitoylated peptides and provides extensive sequence coverage both of the cytoplasmic and transmembrane domains of integral membrane proteins. Using a complementary acyl switch method, we present evidence that DHHC3 is palmitoylated at the DHHC cysteine. We report that DHHC3 binds zinc with a 2:1 zinc/protein stoichiometry and provide biochemical evidence that the highly conserved cysteines within the DHHC3-CRD are required for the structural integrity of the enzyme.

Experimental Procedures

Reagents—Anti-GODZ (DHHC3) antibody was purchased from Millipore, AB9556). M2 FLAG antibody was purchased from Stratagene. Streptavidin-FITC antibody was purchased from Jackson ImmunoResearch Laboratories (West Gove, PA). A ×1000 protease inhibitor mixture of 5 mg/ml leupeptin (Sigma-Aldrich), 1–3 mg/ml aprotinin (Sigma-Aldrich), 1 M PMSF (MP Biomedicals, LLC, Solon, OH), and 1 mM pepstatin A (Amresco, Solon, OH) was mixed from individual components. Trypsin was purchased from Worthington and diluted in 1 mM HCl prior to use. Alexa Fluor® 488 azide was purchased from Invitrogen. *N*-Ethylmaleimide was purchased from Thermo Scientific. Iodoacetamide and 1,10-phenanthroline monohydrate were purchased from Sigma-Aldrich. EZ-link™ biotin-HPDP was purchased from Pierce. Proteinase K from *Tritirachium album* was purchased from Sigma-Aldrich. [^{3}H]palmitoyl-CoA was synthesized as described previously (21, 22).

Constructs—To generate the DHHC3 wild type (WT)-FLAG/His baculovirus, the open reading frame of mouse DHHC3 was ligated to oligonucleotides encoding the appropriate epitopes. The ligated construct was subcloned into pFastbac1 (Invitrogen), yielding pML1627. All FLAG/His-tagged mutants of DHHC3 were created from this plasmid using QuikChange®. The pML1627 plasmid (or its derivatives) was then recombined with bacmid DNA using the Bac-to-Bac baculovirus expression system (Invitrogen) and transfected into Bacvector Sf9 cells (Novagen) using Cellfectin® II. Viruses were amplified to high titer stocks in TriEx Sf9 cells (Novagen) and stored at 4 °C in ESF 921 medium (Expression Systems, Davis, CA) with 10% FBS. The DHHC3–3×Myc/10×His construct was generated by ligating the DHHC3 ORF and a double-stranded oligonucleotide encoding the epitope tags into the pBluebac4.5C(−) vector (Invitrogen). A baculovirus was then generated from this construct using the Bac-N-Blue™ baculovirus expression system.

Acyl-Biotin Exchange (ABE) Assay—TriEx Sf9 insect cells expressing DHHC3 WT or mutants were disrupted in lysis buffer (50 mM HEPES, pH 7.4, 0.5% SDS) containing 50 mM *N*-ethylmaleimide to block free cysteine thiols. DNA was fragmented by passaging the lysate through a 25-gauge syringe needle at least 10 times. The lysate was then cleared by ultracentrifugation at 150,000 × *g* for 20 min. In order to enrich and immobilize DHHC3, the cleared lysate was combined with 30 μl of 50% Ni-NTA resin and rotated for 1 h. The resin was then pelleted; washed three times with 50 mM HEPES, pH 7.4, 0.5% SDS; and divided into two aliquots. DHHC3 was eluted, palmitate was removed, and newly exposed cysteines were alkylated by rotating Ni-NTA resin with elution buffer containing 50 mM HEPES, pH 7.4, 500 mM imidazole, 0.8 mM biotin-HPDP, and a 0.5 M concentration of either neutral HA or NaCl for 2 h at room temperature. Following acetone precipitation, DHHC3, suspended in sample buffer, was resolved by SDS-PAGE and blotted with FITC-streptavidin to detect biotinylation levels and anti-M2 FLAG antibody to detect protein levels. Immunoblots were imaged in a VersaDoc™ 5000 system, and relative signal intensities were quantified using QuantityOne software.

Direct Detection of Palmitate by Mass Spectrometry—Affinity-purified DHHC3 protein samples (4 μg) were separated by a 10% SDS gel and stained by Coomassie Blue R250. The DHHC3 bands were excised, cut into ~1-mm cubes, and subjected to in-gel reduction with 2 mM tris(2-carboxyethyl) phosphine (TCEP), alkylation at 10 mM iodoacetamide, and digestion by trypsin at 35 °C overnight. In-gel extraction of tryptic peptides was conducted as reported previously (23), and extracted peptides were reconstituted in 30 μl of 5% acetonitrile (ACN), 0.5% formic acid (FA) for subsequent nano-LC-MS/MS analysis on an LTQ-Orbitrap Velos (Thermo Fisher Scientific) mass spectrometer-equipped "CorConneX" nano-ion source device (CorSolutions LLC, Ithaca, NY). The nano-LC was carried out by an UltiMate3000 RSLCnano system (Thermo/Dionex, Sunnyvale, CA). The tryptic peptides (5 μl) were injected at a 20-μl/min flow rate onto a tandem trapping column in which a PepMap C4 trap column (5 μm, 300 μm × 5 mm; Thermo) and a PepMap C18 trap column-nanoViper (5 μm, 100 μm × 2 cm; Thermo) were sequentially connected on the nano-HPLC switch valve for loading digested peptides on both trapping columns depending on their hydrophobicity. The trapped peptides in C4 trapping alone were switched to and separated on a downstream in-house-packed C4 nano-column (75-μm inner diameter × 15 cm, 5-μm particles), which was installed on a CorSolution Nano-device with a 10-μm spray emitter (NewObjective, Woburn, MA). The C4-retained peptides were eluted with a 60-min gradient of 10–72% ACN in 0.1% FA at a flow rate of 300 nl/min, followed by a 5-min ramping to 86% ACN, 0.1% FA and a 5-min hold at 86% ACN, 0.1% FA. Peptides retained on the C18 trapping column were analyzed on a downstream C18 nano-column in a separate MS/MS run with a 60-min gradient of 8–38% ACN in 0.1% FA followed by a 5-min ramping to 80% ACN in 0.1% FA. The Orbitrap Velos was operated in parallel data-dependent acquisition mode using a Fourier transform (FT) mass analyzer for one survey MS scan of precursor ions followed by MS/MS scans on the 10 highest intensity peaks with multiple charged ions above a threshold ion count of 7,500 in both an LTQ mass analyzer and high energy collision dissociation-based FT mass analyzer at 7,500 resolution. MS survey scans were at a resolution of 60,000 (full width at half-maximum at m/z 400) for the mass range of m/z 375–1800. All data were acquired under Xcalibur version 2.1 operation software (Thermo Fisher Scientific). MS and MS/MS raw spectra were processed using Proteome Discoverer version 1.4 (Thermo), and the spectra from each data-dependent acquisition file were output as an MGF file for subsequent database search using Mascot version 2.3.02 (Matrix Science, Boston, MA) against the mouse RefSeq database. The database search

was performed with two missed cleavage sites by trypsin allowed. The peptide tolerance was set to 10 ppm, and MS/MS tolerance was set to 0.8 Da for CID and 0.05 Da for high energy collision dissociation. Variable modifications used in database searches include methionine oxidation, deamidation on asparagines/glutamine residues, palmitoylation, and carbamidomethylation on cysteine residue. All spectra of peptides with modified Cys-palmitoylation were manually inspected and confirmed by Xcalibur version 2.1.

Acyl-Iodoacetamide Switch Protocol for Mass Spectrometry Analysis—An acyl switch protocol to prepare samples for mass spectrometry was performed as described for the ABE assay with minor changes. DHHC3 was eluted, palmitate was removed, and newly exposed cysteines were alkylated by rotating Ni-NTA with elution buffer containing 50 mM HEPES, pH 7.4, 0.25% SDS, 500 mM imidazole, 50 mM iodoacetamide, and 0.5 M neutral HA for 2 h at room temperature in the dark. Following precipitation, DHHC3 suspended in sample buffer was resolved by SDS-PAGE. The DHHC3 band was detected with Coomassie Blue staining, excised, and cut into ~1-mm cubes. The protein was digested in gel with trypsin, and proteolytic peptides were extracted as described above. The peptides were reconstituted in 30 μl of 2% ACN with 0.5% FA, and about 100–200 ng of tryptic digests were loaded onto a PepMap C18 trap column-nanoViper (5 μm, 100 μm × 2 cm; Thermo/Dionex) at a 20-μl/min flow rate and then separated on a PepMap C18 reversed phase nano-column (3 μm, 75 μm × 25 cm; Thermo) for nano-LC-electrospray ionization-MS/MS analysis, on an LTQ-Orbitrap Elite mass spectrometer (Thermo Fisher Scientific). The peptides were eluted with a 90-min gradient of 5–38% ACN in 0.1% FA at a flow rate of 300 nl/min, followed by a 7-min ramping to 95% ACN, 0.1% FA and a 7-min hold at 95% ACN, 0.1% FA. Similarly, the Orbitrap Elite instrument was operated in data-dependent acquisition under FT-ion trap acquisition mode using an FT mass analyzer for one survey MS scan of precursor ions followed by MS/MS scans on the 15 highest intensity peaks with normalized collision energy of 35%. All acquired MS and MS/MS raw spectra were processed as described above, except *N*-ethylmaleimide modification of cysteine was included in the database search. All spectra of peptides with carbamidomethyl cysteine were manually inspected and confirmed by Xcalibur version 2.1.

Two-step Purification of DHHC3—TriEx Sf9 insect cells expressing DHHC3-FLAG-His WT or DHHC3 mutants were disrupted in lysis buffer (50 mM Tris, pH 7.4, 200 mM NaCl, 1% *n*-dodecyl-β-D-maltoside (DDM), 10% glycerol, 1 mM TCEP, and protease inhibitors). Cleared lysate was then passed three times through an equilibrated 0.5-ml column of Ni-NTA resin, washed with 40 column volumes of lysis buffer and 30 column volumes of lysis buffer containing 15 mM imidazole. Nickel elutions 1 and 2 were performed by applying 1 column volume of elution buffer containing 50 mM Tris, pH 7.4, 100 mM NaCl, 0.25 mM TCEP, 10% glycerol, 0.1% DDM, and 200 mM imidazole. The imidazole concentration was increased to 500 mM for elutions 3–6. For each elution, the resin was incubated for 10 min in buffer. Elutions were pooled and rotated with ANTI-FLAG® M2-agarose affinity gel (Sigma) equilibrated with Buffer A (50 mM Tris, pH 7.4, 100 mM NaCl, 10% glycerol, 0.1% DDM, 1 mM EDTA, 5 μg/ml leupeptin, and 1 μM pepstatin A) at 4 °C for 2 h. The FLAG affinity resin was washed five times with a total of 50 column volumes of Buffer A and eluted with 5 × 1 column volumes of Buffer A + 0.3 mg/ml FLAG peptide (Sigma). The concentration of enzyme was determined by plotting elution samples along a linear curve generated with known concentrations of bovine serum albumin stained with SYPRO® Ruby protein gel stain (Lonza, Rockland, ME) and quantified using a VersaDoc™ 5000 imaging system.

Protein Acyl Transferase (PAT) Assay—Purified DHHC3 (20–30 nM) was assayed in a 50-μl reaction with 1 μM [^{3}H]palmitoyl-CoA and 1 μM myristoylated $G\alpha_i$ at 25 °C for 6 min. The reaction was stopped with the addition of 5× sample buffer containing 10 mM TCEP. Equal amounts of each reaction were resolved on duplicate Coomassie-stained gels. One gel was soaked for 30 min at room temperature in 1 M salicylic acid and 15% methanol, dried, and exposed to film at −70 °C for fluorographic analysis. The substrate bands in the other gel were excised, cut into ~1-mm cubes, and combined with 500 μl of Soluene 500 (PerkinElmer Life Sciences). The excised gel bands were then heated at either 37 °C overnight or 50 °C for 3 h before being combined with 4.5 ml of Ultima Gold scintillation fluid (PerkinElmer Life Sciences) and counted in a scintillation counter.

Transpalmitoylation Assay—TriEx Sf9 cells were plated on 60-mm dishes and co-infected with two baculoviruses to co-express WT and mutant forms of DHHC3. The DHHC3 WT construct was C-terminally tagged with three Myc epitopes and 10 histidines. The mutant DHHC3 was hexahistidine- and FLAG-tagged. After 48 h of infection, cells were collected and lysed in buffer containing 20 mM Tris, pH 7.4, 300 mM sucrose, 1 mM EDTA, and protease inhibitors, using a ball bearing homogenizer. The membrane fraction of the lysate was isolated by centrifugation and suspended in lysis buffer with a 25-gauge syringe needle. Each membrane preparation was normalized by total protein concentration and DHHC3 content. Equal amounts of membranes were combined with [^{3}H]palmitoyl-CoA at 1 μM final concentration and incubated at 25 °C for 10 min. The reactions were stopped with the addition of 5× sample buffer. Equal amounts of the reaction were resolved on duplicate SDS-polyacrylamide gels. One gel was immunoblotted with anti-DHHC3 antibody to detect protein levels of WT and mutant enzymes. The other gel was fixed in 40% methanol and 10% acetic acid, stained with Coomassie Blue, and processed for fluorography.

Limited Proteolysis Assay—Purified WT DHHC3 and DHHC3 mutants were buffer-exchanged into 50 mM Tris, pH 7.4, 100 mM NaCl, 10% glycerol, 1 mM EDTA, and 2 mM TCEP using Sephadex G25 size exclusion resin. DHHC3 was combined with trypsin at a 10:1 ratio and incubated on ice for 45 min. The reaction was stopped with 1× protein sample buffer and a 10-fold excess of soybean trypsin inhibitor. The reactions were resolved by SDS-PAGE for immunoblots with anti-DHHC3 antibody (Millipore).

Chemical Treatment of DHHC3—TriEx Sf9 insect cells (5 × 10^6 cells) were infected with baculovirus encoding DHHC3 WT and incubated with 0.5 mCi of [^{3}H]palmitate for 2 h. Radiolabeled DHHC3 WT protein was isolated on Ni-NTA resin under

non-denaturing conditions. DHHC3 was eluted in 50 mM Tris, pH 7.4, 100 mM NaCl, 0.1% DDM, and 500 mM imidazole. The elution was buffer-exchanged into 50 mM Tris, pH 7.4, 100 mM NaCl, 10% glycerol, 0.05% DDM, 2 mM TCEP, and 1 mM EDTA using Sephadex G25 size exclusion resin. The eluate from the size exclusion resin was then aliquoted into separate reactions. Each aliquot of protein was exposed to HA, DTT, TCEP, or 1,10-phenanthroline at the concentrations shown in Fig. 6 or with H_2O as a control and incubated at 25 °C for 60 min. The reactions were then buffer-exchanged to remove treatment reagents. PAT activity and the limited proteolysis pattern of DHHC3 from each reaction were evaluated as described above. To measure removal of palmitate by the chemical treatments, an aliquot of the reaction was subjected to SDS-PAGE and processed for fluorography and assayed for protein levels by immunoblot. Radiolabeled protein was quantitated by densitometry and normalized to protein levels in the immunoblot.

Zinc Measurement and Detection—Measurement of zinc was performed on recombinant DHHC3 that was tagged only with the FLAG epitope to avoid any spurious metal binding from a histidine tag. Insect cells expressing DHHC3-FLAG were lysed with buffer containing 20 mM HEPES, pH 7.2, 200 mM NaCl, 10% glycerol, 1% DDM, and protease inhibitors. The cell lysate was cleared by ultracentrifugation at 150,000 × *g* for 20 min at 4 °C, and the supernatant was applied to ANTI-FLAG® M2-agarose affinity gel (Sigma). After washing with 80 column volumes of wash buffer (20 mM HEPES, pH 7.2, 200 mM NaCl, 10% glycerol, 0.1% DDM) with protease inhibitors and 20 column volumes of wash buffer without protease inhibitors, DHHC3 was eluted with 5 × 1 column volumes of wash buffer without protease inhibitors + 0.1 mg/ml FLAG peptide (Sigma). Purified DHHC3 was then applied to a preparative size exclusion column (SEC), using wash buffer without protease inhibitors as the mobile phase. Fractions containing a monodispersed DHHC3 peak were collected, pooled, and analyzed by fluorescent size exclusion chromatography (24). To evaluate metal ions bound by DHHC3, aliquots of purified DHHC3 were digested with proteinase K overnight at 56 °C and then heated at 90 °C for 10 min. After cooling to room temperature, the digested protein sample was combined with 8–16 μM mag-fura-2 (final). Fluorescence emission at 505 nm was monitored while exciting the solution with a spectrum of wavelengths from 300 to 400 nm. The concentration of free zinc ions was calculated from the ratio of fluorescence emitted at the excitation wavelengths 325 and 350 nm (25). This ratio was then plotted against a standard curve of 325 nm to 350 nm ratios derived from known zinc concentrations generated with an atomic absorption standard of zinc oxide (Fisher). The zinc standard was serially diluted in H_2O and added to the same buffer and proteinase K mixture as present in experimental samples. All standard curves were generated and heated in parallel with experimental samples. The protein content of the samples was measured against a standard curve of commercial BSA standards (2 ± 0.03 mg/ml; Pierce) serially diluted in wash buffer without protease inhibitors. The BSA standard curve and experimental samples were resolved on SDS-polyacrylamide gels and stained with SYPRO® Ruby protein gel stain (Lonza, Rockland, ME) and quantified using a VersaDoc™ 5000 imaging system.

Results

Identification of Palmitoylated Cysteines in the CRD of DHHC3—We used mass spectrometry to identify the sites of palmitoylation of DHHC3. Mass spectrometry offers the most accurate and direct means of identifying palmitoylation sites in proteins. However, standard tandem mass spectrometry analysis with upstream reversed phase liquid chromatography (LC-MS/MS) has traditionally struggled to directly identify lipid modifications of proteins because hydrophobic interactions between lipid modifications and the commonly used C18 reversed phase HPLC column are frequently too strong to enable elution of lipidated peptides prior to MS/MS analysis (26).

We directly identified two palmitoylated cysteines in DHHC3 using a C4-based LC-MS/MS method. DHHC3 was purified from insect cells and resolved by SDS-PAGE. An in-gel trypsin digestion was performed, and DHHC3 peptides were applied to a C4 trapping column and a C18 trapping column connected in series. The most hydrophobic and palmitoylated peptides were retained on the C4 column, whereas less hydrophobic peptides flowed through and were trapped on the C18 column. The C4 and C18 trapping columns were then individually connected to a C4 nanocolumn and a C18 nano-column, respectively, in two separate LC-MS/MS runs. Using this combined C4 and C18 chromatography method, peptides accounting for 72% sequence coverage of DHHC3 were confidently identified in the MS/MS data, including three of the four transmembrane domains (Fig. 1*A*, *solid line*). With the exception of the tripeptide containing Cys-149, the entire sequence of the DHHC-CRD was recovered. No palmitoylation was detected on Cys-129, -132, -143, -157, and -163. Palmitate was directly and reproducibly observed on cysteine 146, and in one repetition, palmitate was also observed on cysteine 133 (Fig. 1*B*).

We were surprised not to find palmitate on the DHHC cysteine, the postulated site of autoacylation. Palmitate could be lost from DHHC3 during sample preparation due to the susceptibility of thioester-linked palmitate to hydrolysis (26). Accordingly, we employed a complementary method to identify additional palmitoylation sites on DHHC3. An acyl switch protocol was used to replace palmitate with iodoacetamide on DHHC3, thereby rendering peptides more easily recovered using standard C18 reversed phase HPLC prior to tandem mass spectrometry. The carbamidomethyl modification of DHHC3 is more stable than thioester-linked palmitate (26). MS/MS analysis of the acyl switch processed DHHC3 identified iodoacetamide at Cys-24, -132, -133, -157, and -163 (Fig. 1*C*). Iodoacetamide at the DHHC cysteine (Cys-157) was detected in 11 of the 13 identifications of the peptide. These results represent the first report of palmitate at the cysteine in the DHHC motif, strengthening support for this residue as the site of autoacylation in the acyl-enzyme intermediate. The observation of iodoacetamide on Cys-133 is consistent with the results of our direct detection of palmitate on this residue. However, we did not observe the Cys-146 peptide, modified or unmodified, in either the MS or the MS/MS data in this analysis, indicating

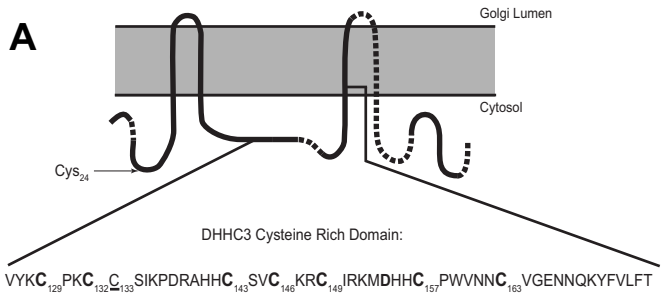

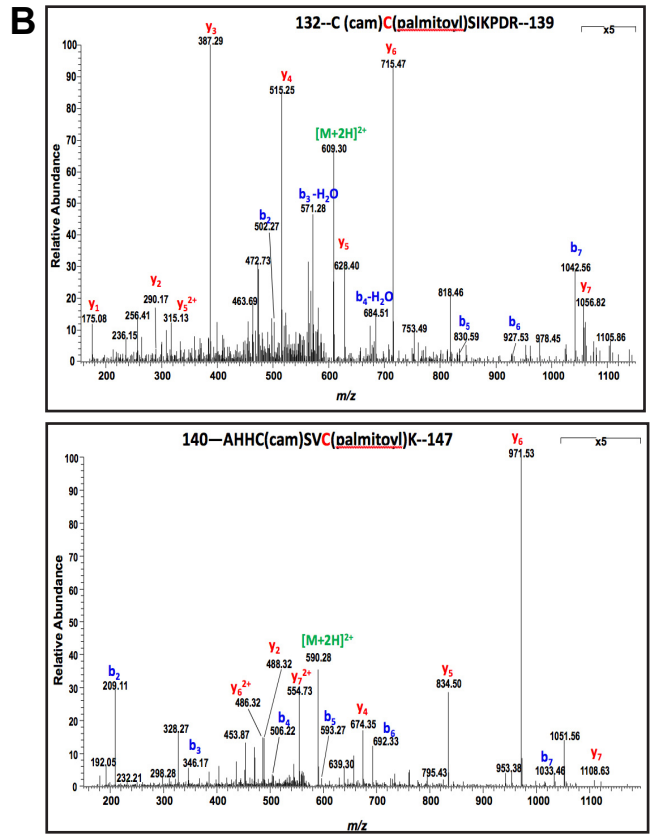

C

Peptide sequence	IAA modified / Total Identifications	
CAPPPFPGPAGAMWFIR		
$C24_{IAA}$	7 / 62	11%
CCSIKPDR		
$C132_{IAA}$ + $C133_{IAA}$	7 / 16	44%
MDHHCPWVNNCVGENNQK		
$C157_{IAA}$ + $C163_{NEM}$	5 / 13	38%
$C157_{IAA}$ + $C163_{IAA}$	6 / 13	46%

FIGURE 1. **Multiple palmitoylated cysteines in DHHC3 can be identified by mass spectrometry.** *A*, diagram of the predicted topology of DHHC3. The portions drawn with a *solid line* indicate sequence coverage observed with the tandem C4-C18 LC/MS/MS method described under "Experimental Procedures." The CRD sequence is displayed *below*, with highly conserved cysteines in *boldface type*. The location of unconserved cysteines 24 (*arrow*) and 133 (*underlined*) is indicated. *B*, direct MS/MS identification of DHHC3 palmitoyl-peptides from a tryptic digest of DHHC3 purified from insect cells. A mass shift (238.2300 atomic mass units) was identified on Cys-133 and Cys-146 corresponding to the molecular weight of palmitate. *C*, peptides identified in the MS/MS analysis of an acyl switch assay performed on DHHC3 purified from insect cells. Unmodified cysteines were blocked with *N*-ethylmaleimide, and palmitate was replaced with iodoacetamide (*IAA*) in a hydroxylamine-dependent manner. The frequency of carbamidomethyl (iodoacetamide-modified) cysteine identifications, relative to total peptide identifications, is listed. Carbamidomethyl-Cys-157 was identified in 11 out of 13 identified peptides observed in this analysis.

that the peptide was not recovered following the in-gel digest for unknown reasons. Peptides containing two other conserved cysteines within the CRD, Cys-129 and Cys-149, were not detected due to their small size. Accordingly, we could not exclude these residues as potential palmitoylation sites.

Taken together, the mass spectrometry analysis identified four of the seven conserved cysteines in the CRD (Cys-132, Cys-146, Cys-157, and Cys-163), an unconserved cysteine in the CRD (Cys-133), and an unconserved cysteine in the unique N-terminal domain of DHHC3 (Cys-24) as palmitoylation sites. To understand the conserved role of palmitoylation in DHHC protein function, we focused on the cysteine residues in the CRD for further study.

Mutation of the DHHC Cysteine, Cys-157, or a Conserved Cysteine, Cys-146, Reduces Palmitoylation of DHHC3 in Cells—We predicted that mutation of palmitoylation sites would reduce the overall palmitoylation level of the enzyme. To test this, we individually mutated each CRD cysteine in DHHC3 to serine and assayed the relative palmitoylation level of each construct by acyl-biotin exchange. We included all of the conserved cysteine residues in the DHHC-CRD and the unconserved Cys-133 in our analysis. Mutation of Cys-143, Cys-149, and Cys-163 produced enzymes that could not be retained on the Ni-NTA resin used to isolate the DHHC proteins in these assays, probably indicating that mutation at these sites results in a misfolded protein. Therefore, DHHC3(C143S), DHHC3(C149S), and DHHC3(C163S) were not analyzed further.

In the ABE assays, mutation of the DHHC cysteine, Cys-157, resulted in the loss of nearly all of the palmitate on DHHC3 (Fig. 2, *A* and *B*), consistent with published work (12, 27). Mutation of Cys-146 also significantly decreased DHHC3 palmitoylation, consistent with our direct identification of palmitate at Cys-146 by mass spectrometry. However, DHHC3 palmitoylation was unaffected by mutation of Cys-129, Cys-132, or Cys-133. The apparent low stoichiometry of palmitoylation suggests that these are spurious sites of palmitoylation identified through the sensitivity of the mass spectrometry methods.

Mutation of Conserved Cysteines in the CRD Results in Activity Deficits—We next addressed the functional importance of the conserved cysteines in the CRD with respect to enzyme activity. DHHC3 and CRD cysteine mutants were purified to near homogeneity and assayed for PAT activity. The amount of palmitate transferred to $G\alpha_i$ was analyzed by liquid scintillation counting of the excised substrate band (Fig. 3*A*) and by fluorography (Fig. 3*B*). Spontaneous palmitoylation of $G\alpha_i$ in these reactions was quantified using an enzyme-free reaction (shown in Fig. 3*B*, *lane 1*) and subtracted from total substrate palmitoylation observed in enzymatic reactions (Fig. 3*A*).

As anticipated (11), the DHHS3(C157S) was catalytically inactive. Mutation of the other three conserved cysteines either rendered the enzyme inactive (C132S) or markedly reduced enzyme activity (C129S or C146S). By contrast, mutation of the unconserved Cys-133 retained activity comparable with the WT enzyme (Fig. 3*A*). Fluorography analysis showed that the

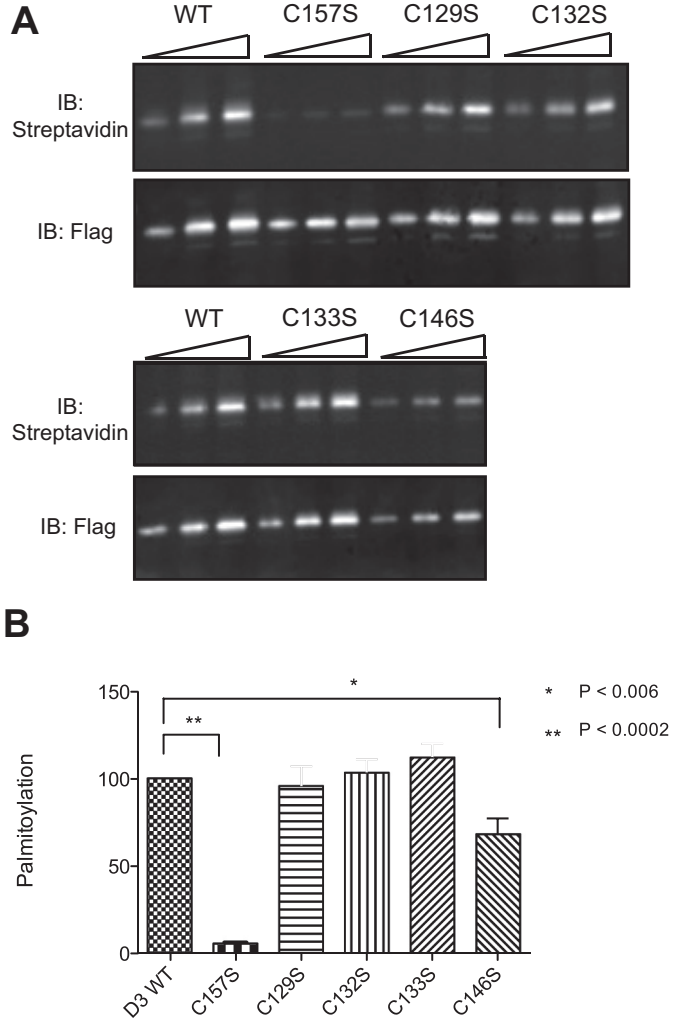

FIGURE 2. **Mutation of cysteines 146 and 157, but not other CRD cysteines, reduces the palmitoylation level of DHHC3 in cells.** *A*, total palmitoylation levels of purified DHHC3 WT and DHHC3 mutants were detected using acyl-biotin exchange. Palmitate on DHHC3 was replaced with biotin-HPDP in a hydroxylamine-dependent manner. Increasing amounts of each construct were resolved by SDS-PAGE in order to compare the signal from different constructs. Biotinylated DHHC3 was then blotted for both total protein (*IB*: *Flag*) and for biotinylation levels (*IB*: *streptavidin*). *B*, the average streptavidin signals from the best-normalized amounts of each construct are displayed. Mutation of Cys-146 and Cys-157 reduced palmitoylation of DHHC3, as indicated by streptavidin-FITC signals. Mean and S.E. (*error bars*) are shown for three or four experiments for each protein, and *p* values were calculated using two-tailed Student's *t* tests.

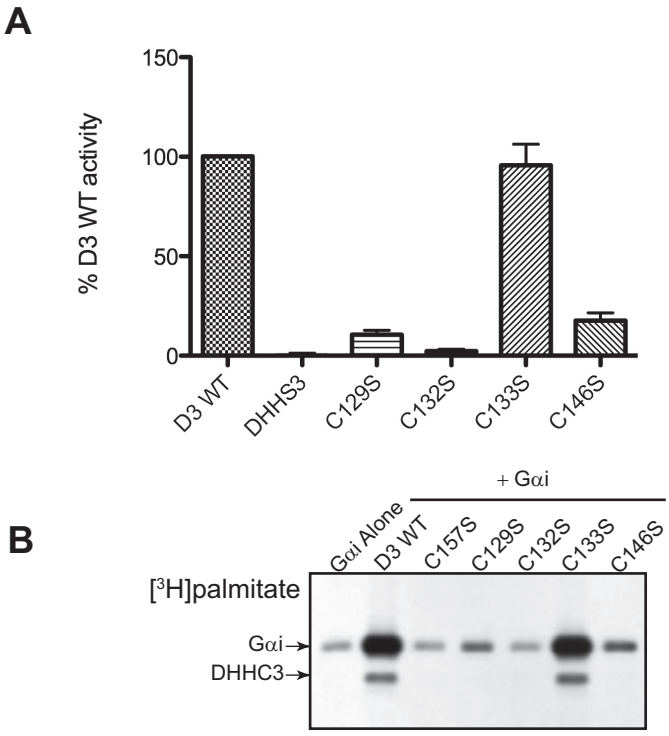

FIGURE 3. **Mutation of conserved cysteines in the CRD results in PAT activity deficits.** PAT activity of purified DHHC3 WT and cysteine mutant proteins was assayed by combining 20–30 nM purified enzyme with 1 μM [^{3}H]palmitoyl-CoA and 1 μM myristoylated Gα_i as a protein substrate. *A*, [^{3}H]palmitate transferred to Gα_i was measured by liquid scintillation counting as described under "Experimental Procedures." Non-enzymatic acylation of Gα_i was measured in the absence of DHHC3 and subtracted from reactions containing enzyme. Enzyme activity was normalized to WT DHHC3. Mean and S.E. (*error bars*) are shown for 3–5 experiments for each mutant protein assayed. *B*, fluorography analysis demonstrates that both autoacylation (*DHHC3 band*) and transfer activity (*Gα_i band*) are reduced in conserved cysteine mutants (C157S, C129S, C132S, and C146S) but not in the unconserved C133S mutant. Results are representative of at least three experiments.

strength of autoacylation in DHHC3 mutants was proportional to their transfer activity (Fig. 3*B*). These results demonstrate that at least four conserved cysteines in the CRD of DHHC3 are required to support efficient catalytic activity of the enzyme.

Transpalmitoylation Assays Suggest That the Mutation of Conserved Cysteines Disrupts the Tertiary Structure of DHHC3—DHHC3 has been shown to form oligomers in cells and *in vitro* (22, 28). We investigated whether DHHC3 monomers can palmitoylate each other in *trans*, as a functional aspect of their oligomeric state. To do so, we assayed PAT activity in membranes from cells co-expressing WT DHHC3 and various mutants. To distinguish the electrophoretic mobility of DHHC3 from the mutant enzymes, the WT protein was epitope-tagged with a longer sequence than the mutant enzymes. Consistent with a previous study of the yeast DHHC protein Akr1 (14), we found that when DHHS3(C157S) is co-expressed with DHHC3 WT, we could detect *in vitro* palmitoylation of DHHS3 (C157S) (Fig. 4, *lane 4*). We then asked whether mutation of CRD cysteines in the context of DHHS3(C157S) would result in a reduction of transpalmitoylation. We constructed double mutant forms of DHHC3 in which Cys-157 was mutated in combination with a second cysteine residue in the CRD. Surprisingly, increased transpalmitoylation of the mutants was seen when a conserved CRD cysteine (Cys-129, Cys-132, or Cys-146) was mutated in combination with Cys-157 (Fig. 4, *A* (*lower bands*) and *B*). By contrast, transpalmitoylation of the C157S/C133S double mutant was similar to that of the C157S single mutant. Thus, increased transpalmitoylation of conserved cysteine mutants correlates with reduced or absent PAT activity. We hypothesized that mutation of the conserved cysteines (Cys-129, Cys-132, and Cys-146) in the context of the DHHS (C157S) mutant causes a structural change in the CRD that exposes previously inaccessible cysteines for ectopic palmitoylation by the coexpressed WT protein.

Limited Proteolysis Assays Identify Structural Perturbations in Conserved CRD Cysteine Mutants of DHHC3—To investigate whether mutation of conserved cysteines other than the

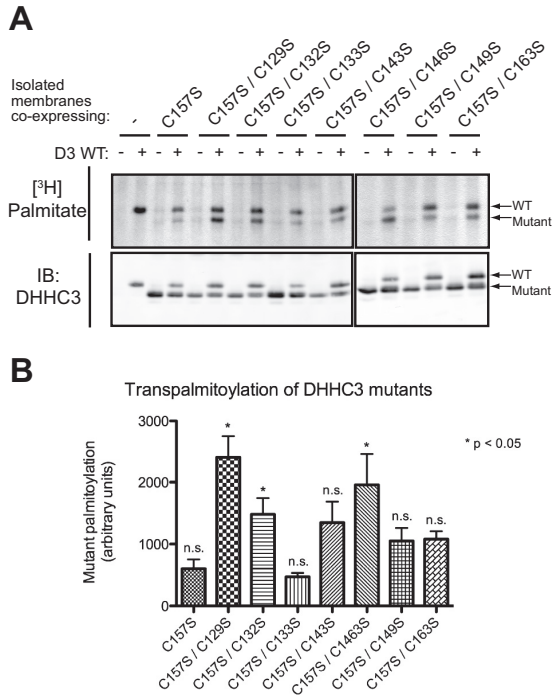

FIGURE 4. **Transpalmitoylation assays suggest that the mutation of conserved cysteines disrupts the tertiary structure of DHHC3.** *A*, membranes were isolated from Sf9 insect cells expressing a mutant DHHC3-FLAG/His_6 protein (*bottom band*) alone or in combination with a Myc_3/His_{10}-tagged DHHC3 WT protein (*higher molecular weight band*). Isolated membranes were normalized for total protein and combined with 1 μM [^{3}H]palmitoyl-CoA (final). The *top panel* shows a representative fluorographic analysis of the amount of [^{3}H]palmitate accumulated on WT and mutant DHHC3. Protein levels of DHHC3 are displayed in the immunoblot (*bottom*). Results are representative of at least three experiments. *B*, densitometry analysis of the average fluorography band produced by each mutant DHHC3 protein when palmitoylated in *trans* by DHHC3 WT. *Error bars*, S.E. for at least three experiments; *, $p < 0.05$, resulting from a two-tailed Student's *t* test comparing each double mutant with the C157S single mutant.

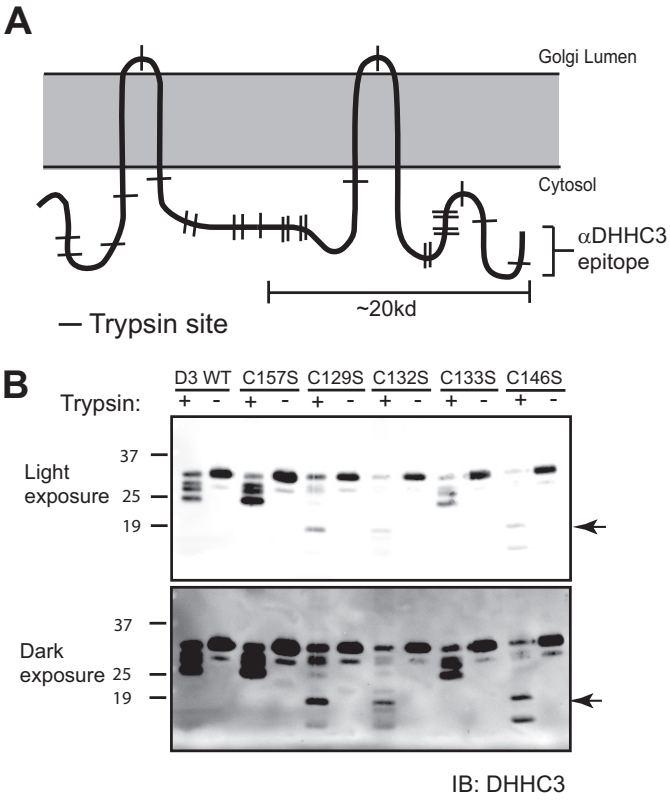

FIGURE 5. **Limited proteolysis assays identify structural perturbations in conserved CRD cysteine mutants of DHHC3.** *A*, diagram of the predicted topology of DHHC3. The approximate locations of potential trypsin cleavage sites are marked with *perpendicular lines*. The location of the DHHC3 antibody epitope is indicated. *B*, purified WT DHHC3 or single cysteine mutants of DHHC3 were combined with trypsin and incubated on ice for 45 min. The reactions were stopped with sample buffer containing soybean trypsin inhibitor and resolved by blotting with an antibody raised against the C-terminal 15 amino acids of DHHC3 (29). Partial proteolysis of DHHC3 mutants C129S, C132S, and C146S produces a ~20-kDa fragment (*arrowhead*) that is absent in the proteolytic patterns of DHHC3 WT, DHHS3(C157S), and DHHC3(C133S). Results are representative of at least three experiments. *IB*, immunoblot.

DHHC cysteine perturbed the structure of DHHC3, we performed limited proteolysis experiments on purified DHHC3 WT and CRD cysteine mutants. Proteolytic fragments produced in these experiments were resolved by SDS-PAGE and detected in immunoblots with an antibody raised against the C-terminal 15 amino acids of DHHC3 (29). In DHHC3 WT, DHHS3(C157S), and DHHC3(C133S) mutants, the enzyme was digested preferentially from the N terminus, producing proteolytic bands immediately below the parental band. By contrast, limited proteolysis of C129S, C132S, and C146S mutants produced a ~20-kDa fragment (Fig. 5*B*). The size of the fragment is consistent with exposure of a previously inaccessible trypsin site in the CRD of DHHC3 (Fig. 5*A*). The difference in proteolytic patterns observed between the C157S mutant and other conserved cysteine mutants supports the results of our transpalmitoylation assays, suggesting that the CRD of the C157S is tightly ordered, limiting access to most cysteines and trypsin sites. Similarly, the CRD is unaffected in mutation of the unconserved Cys-133. By contrast, mutation of Cys-129, Cys-132, and Cys-146 exposes previously inaccessible portions of the CRD. However, it is unclear from these results whether structural perturbation in these conserved CRD cysteine mutants is related to palmitoylation of the CRD.

Treatment with Chelating Reagents Replicates Characteristics of Conserved CRD Cysteine Mutants—To determine whether there was a role for palmitoylation in structuring the CRD, we sought to chemically remove palmitate from DHHC3 and assay the impact on the limited proteolysis pattern and PAT activity of the enzyme. We expressed DHHC3 WT in insect cells and metabolically labeled the cells with [^{3}H]palmitate to enable subsequent removal of palmitate to be monitored. DHHC3 was then purified and eluted under non-denaturing conditions using Ni-NTA resin. The enzyme was treated with either HA or DTT to remove palmitate and subsequently assayed for PAT activity and proteolytic digestion patterns relative to H_2O-treated DHHC3. In order to control for the reducing and chelating (30) activities of DTT, DHHC3 was also treated with a second chelator, 1,10 phenanthroline, and a second reducing reagent, TCEP, which is not a chelator (31).

As seen in the fluorograph (Fig. 6*A*) and quantified in Fig. 6*B*, HA and DTT, but not TCEP or 1,10-phenanthroline, removed palmitate from DHHC3. However, only DTT and 1,10-phenanthroline-treated DHHC3 replicated the proteolytic digestion pattern of the conserved cysteine mutants (C129S, C132S, and C146S) (compare Fig. 6*B* with Fig. 5*B*). Furthermore, DHHC3

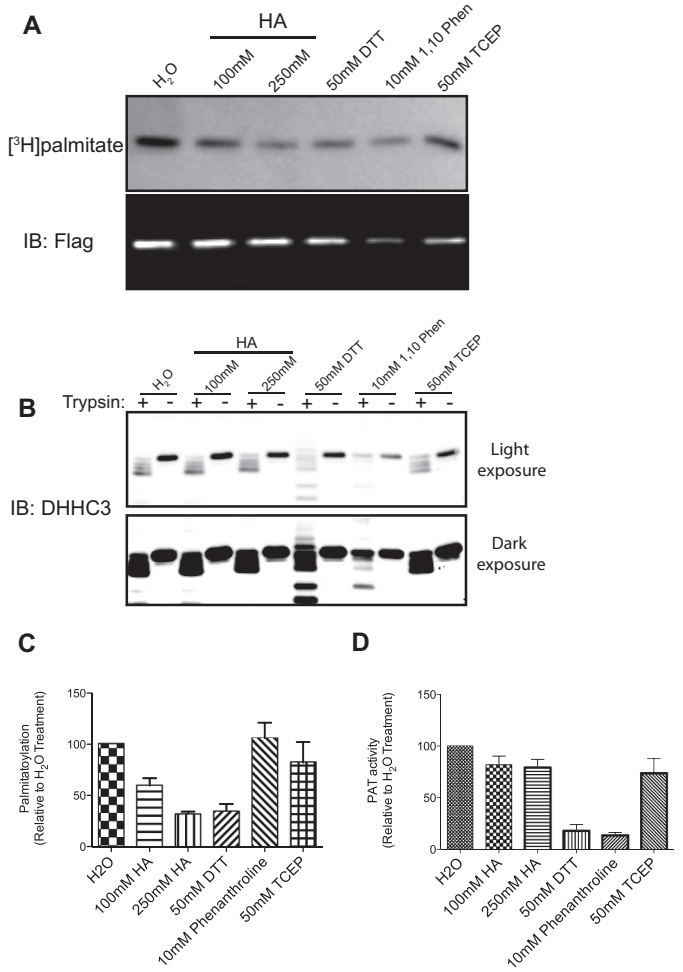

FIGURE 6. **Treatment with chelating reagents replicates characteristics of conserved CRD cysteine mutants.** DHHC3 WT was metabolically labeled with [^{3}H]palmitate in Sf9 insect cells to enable monitoring of palmitate removal. Radiolabeled protein was purified using Ni-NTA resin. Purified protein was buffer-exchanged to remove imidazole and then treated with DTT or two different concentrations of HA to remove palmitate from the enzyme. 1,10-Phenanthroline and TCEP were included to control for the chelating activity and the reducing activity of DTT, respectively. *A*, residual [^{3}H]palmitate labeling following treatment is shown in the *top panel*; an immunoblot (*IB*) of protein levels is displayed *below*. *B*, chemically treated DHHC3 was subjected to limited proteolysis and analyzed by an immunoblot with a DHHC3 antibody. Both a light and dark exposure of the results are presented. Treatment with DTT and 1,10-phenanthroline, but not HA or TCEP, replicates the limited proteolysis pattern of conserved CRD cysteine mutants (C129S, C132S, and C146S) shown in Fig. 5*B*. *C*, quantification of palmitate remaining on DHHC3 post-treatment (normalized to protein), relative to an H_2O-treated control. Mean and S.E. (*error bars*) are shown for three experiments. *D*, the relative activity of DHHC3 following chemical treatment in these experiments is shown. Chemically treated DHHC3 was buffer-exchanged into a non-denaturing buffer suitable for PAT assays and divided into two aliquots. One aliquot was heat-inactivated to control for spontaneous acylation, and the second was held on ice. PAT activity was assayed as described under "Experimental Procedures." Spontaneous acylation was subtracted from the value for each experimental sample. PAT activity of DHHC3 treated with water was set at 100%, and the activities of chemically treated samples were normalized to that value. Mean and S.E. are shown for three experiments.

enzyme activity could not be recovered after treatment with DTT and 1,10-phenanthroline (Fig. 6*D*). By contrast, no dose-dependent impact on enzyme activity was observed as a result of removing palmitate with HA (Fig. 6*D*). These results suggest that the reduced activity and structural perturbations observed in conserved CRD cysteine mutants are the result of destabilized metal ion binding in the CRD of DHHC3 and are independent of enzyme palmitoylation.

Direct Detection of Zinc Binding in Purified DHHC3—The results of our chemical treatment assays indicated that the CRD of DHHC3 included a metal ion-binding motif. To identify the metal ion bound by the CRD of DHHC3, we used the fluorescent zinc indicator mag-fura-2 (Life Technologies) (25). Mag-fura-2 emits fluorescence at 505 nm when excited with a wavelength spectrum from 300 to 400 nm. In the absence of zinc, this emission peaks at an excitation wavelength of 375 nm. In complex with zinc ions, peak emission shifts to an excitation wavelength of 325 nm. In the shift from 375 to 325 nm, mag-fura-2 exhibits an isosbestic point at an excitation wavelength of 350 nm (25). We confirmed that a shift in peak emission from 375 to 325 nm occurred in the presence of zinc but not in the presence of other bioavailable ions at low micromolar concentrations (Fig. 7, *A* and *B*).

To determine whether DHHC3 contained zinc, DHHC3 was purified to near homogeneity using FLAG affinity resin. Purified DHHC3 was then applied to a preparative SEC. Fractions containing a monodispersed population of DHHC3 were collected and pooled (Fig. 7*C*, *shaded area*), whereas fractions containing aggregated or denatured DHHC3 were discarded. Analysis by fluorescent SEC (24) showed the final pool of DHHC3 to be contained in a single monodispersed peak (Fig. 7*D*), suggesting a nearly uniform population of active enzyme. PAT activity of the final DHHC3 pool was confirmed (0.6 pmol of [^{3}H]palmitoyl-Gα_i formed in a 6-min assay).

To assess the zinc content of DHHC3, aliquots of the purified DHHC3 pool were digested with proteinase K overnight. Mag-fura-2 was combined with proteolyzed DHHC3, and fluorescence emission spectra were taken. A standard curve of buffer-matched samples containing proteinase K and known amounts of zinc was processed in parallel. Quantification of zinc in each sample was determined by calculating the ratio of emitted fluorescence at 325 nm relative to 350-nm excitation wavelengths, which increases linearly in relation to increasing zinc concentrations (Fig. 7*B*).

A strong zinc signal was observed in experimental samples, confirming the identity of the metal ion bound by DHHC3. The zinc concentration was 1.99 $\pm$ 0.07 μM ($n = 4$); the protein concentration was 0.97 $\pm$ 0.04 μM ($n = 4$). These values indicate a binding stoichiometry of 2 mol of Zn^{2+}/mol of protein (Fig. 7*D*), suggesting two zinc binding sites in DHHC3. The similarity of the trypsin digestion patterns and loss of enzyme activity that result from zinc chelation and from mutation of Cys-129, Cys-132, or Cys-146 strongly implicate these residues in coordination of zinc. We suggest that Cys-143, Cys-149, and Cys-163 are also likely to have a role in zinc coordination, given the impact of mutation on the structural integrity of these mutant proteins. Our results, thus, are consistent with a model of two CCHC zinc fingers within the CRD of DHHC proteins (19).

Discussion

In this study, we performed a structure/function analysis of the conserved cysteine residues in the cysteine-rich domain of DHHC3. We sought to determine the number and identity of

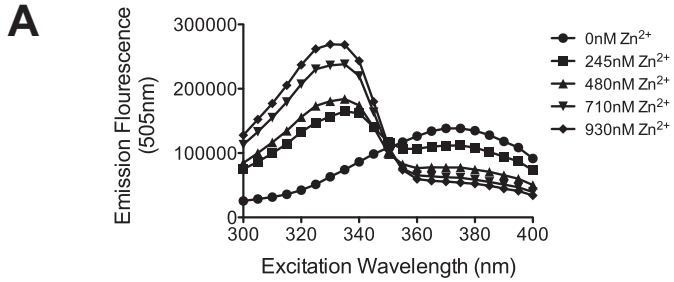

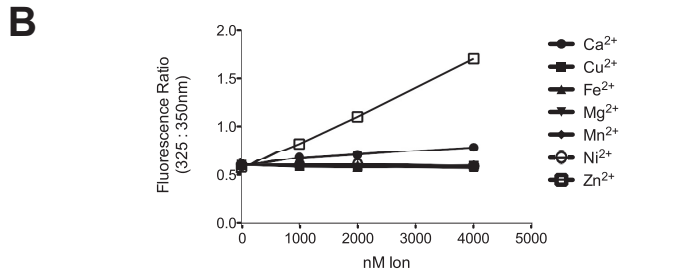

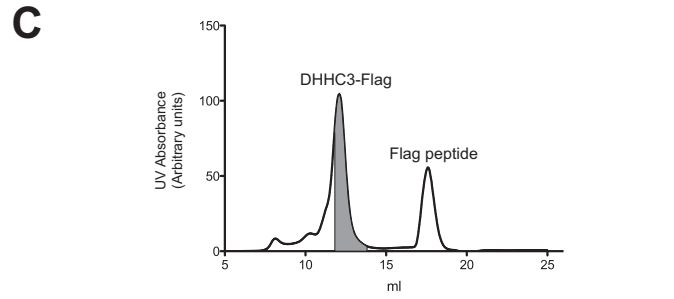

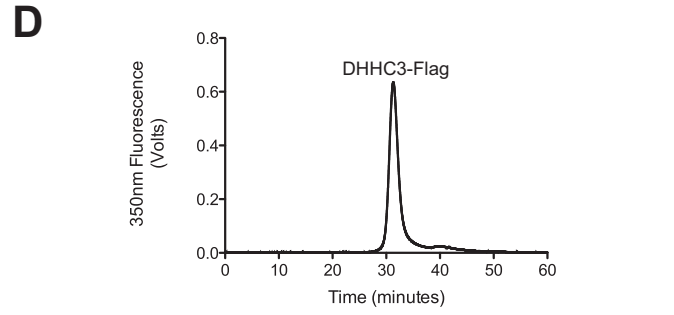

E

D3-Flag concentration	Zn^{2+} concentration
0.97 +/- 0.04μM n=4	1.99 +/- 0.07μM n=4

FIGURE 7. **Direct detection of zinc bound to purified DHHC3.** *A*, the fluorescent zinc indicator mag-fura-2 responds to increasing zinc concentrations by shifting peak fluorescence from 375 to 325 nm on an excitation wavelength spectrum. *B*, at low micromolar ion concentrations, the ratio of fluorescence emitted by mag-fura-2 at excitation wavelengths 325 and 350 nm responds in a positive linear correlation to free Zn^{2+}, very weakly to free Ca^{2+}, and not at all to Cu^{2+}, Fe^{2+}, Mg^{2+}, Ni^{2+}, or Mn^{2+}. *C*, FLAG-tagged DHHC3 was purified to near homogeneity using ANTI-FLAG® M2-agarose affinity gel (Sigma). Elutions were pooled and applied to a preparative SEC. Fractions containing a monodisperse population of DHHC3 (*shaded area under* the *curve*) were selected and pooled. *D*, the pool was confirmed to be monodisperse by applying a sample to an analytical SEC monitored by intrinsic tryptophan fluorescence. To quantify zinc bound to DHHC3-FLAG, aliquots from the monodisperse pool were digested overnight with proteinase K to release zinc from the protein. Free zinc in these samples was detected with mag-fura-2 and compared with a buffer-matched standard curve of known zinc concentrations. *E*, total DHHC-FLAG protein was quantified in parallel samples (minus proteinase K) as described under "Experimental Procedures." The zinc and protein concentrations are reported as concentrations ± S.E. and suggest that each molecule of DHHC3 binds two zinc ions.

the palmitoylation sites in the CRD. Our analysis provided direct evidence that the cysteine of the DHHC motif is palmitoylated, strongly supporting its role as the site of the acyl-enzyme intermediate in the palmitoylation reaction. Several additional cysteines were identified as palmitoylation sites by mass spectrometry, but further studies suggested that these residues are more likely involved in coordinating zinc. We demonstrated that an intact and active DHHC protein is a zinc metalloprotein, confirming earlier work on the isolated Swf1 CRD (19). The model of the Swf1 CRD proposed by González Montoro *et al.* (19) contains two CCHC zinc-binding sites, in which six conserved cysteines coordinate zinc. Our biochemical characterization of DHHC3 mutants is consistent with a similar role for the corresponding cysteines in the DHHC3-CRD.

Structural and Functional Roles of the Cysteines within the CRD—Prior genetic and biochemical studies have established that the DHHC motif is the catalytic core of the DHHC family of PATs (11, 20, 32). *In vitro*, mutation of the cysteine in the DHHC motif abolishes autoacylation and transfer of the fatty acid to a substrate protein. *In vivo*, the same mutation essentially eliminates steady state palmitoylation of the enzyme (12). Thus, it has been long presumed that the DHHC cysteine is at least transiently modified with palmitate. We conclude that our identification of palmitoylation at the DHHC cysteine by mass spectrometry represents an authentic site because the palmitoylated peptide was detected at a significantly higher frequency than that of the other peptides (84% of the peptides recovered; Fig. 1*C*) and is consistent with the ABE analysis of the palmitoylation state of the DHHS(C157S) mutant (Fig. 2). It is also notable that in contrast to the other conserved cysteine residues that we studied, mutation of the DHHC cysteine does not have a noticeable impact on the structural integrity of the enzyme, whereas it clearly has a role in catalysis.

Of the remaining sites of palmitoylation that were identified in DHHC3, the apparent low stoichiometry of palmitoylation (Fig. 2) suggests that these residues are available to coordinate zinc. Cys-146 is the only plausible candidate for a palmitoylation site based on the ABE analysis, which showed a significant reduction of palmitoylation of C146S (Fig. 2). However, the results of the transpalmitoylation (Fig. 4) and limited proteolysis assays (Fig. 5) suggest that many cysteines in the CRD are inaccessible when the enzyme is in its native folded state. As such, our mass spectrometry identification of sites of palmitoylation in the CRD other than the DHHC cysteine is probably an artifact of protein misfolding and ectopic transpalmitoylation.

Zinc-binding cysteines in proteins can serve structural, catalytic, or regulatory roles (33). It is clear that palmitoyltransferases of the DHHC family do not require the zinc finger motifs to be active as PATs. Yeast Akr1, one of the first DHHC proteins to be characterized biochemically as a PAT (27), lacks five of the cysteines and one of the histidines that constitute the two zinc fingers. Our work and that of others support a struc-

tural role for zinc in DHHC proteins. In Swf1, mutation of all of the conserved cysteine and histidine residues assigned to the CCHC zinc fingers results in misfolded proteins and loss of function *in vivo* (19). Similar results have been reported for the yeast DHHC proteins Erf2 (32) and Pfa3 (34), although the impact of mutation is less severe for some residues. In Erf2, mutation of the residue equivalent to Cys-163 in DHHC3 resulted in a partial loss of function *in vivo* and had only a modest effect on enzyme activity *in vitro* (32). Pfa3 tolerated mutation of the cysteines corresponding to Cys-129, Cys-132, or Cys-146 in DHHC3, as assessed by the ability of Pfa3 to palmitoylate its substrate Vac8 in yeast (34). Interestingly, DHHC3 proteins harboring analogous mutations to these sites were amenable to purification and, in two cases, displayed some enzyme activity. Thus, there may be some plasticity in an individual DHHC protein that enables it to tolerate the loss of a cysteine residue that would disrupt one of the zinc fingers.

Identification of Palmitoylation Sites by Mass Spectrometry—Improved proteomic methods have enabled the cataloguing of the palmitoyl proteome from many tissues and cell lines (4). However, there are fewer reports that include identification of the sites of palmitoylation. Yang *et al.* (13) and Forrester *et al.* (35) used variations of acyl switch methods to recover palmitoylated peptides and identify the modified cysteine by mass spectrometry. Development of a method to directly detect palmitoylated peptides is desirable. First, direct detection eliminates false positive identifications associated with incomplete blockage of free cysteine thiols prior to hydroxylamine treatment or with other thioester-linked post-translational modifications. Second, it enables the identification of the fatty acid attached to the cysteine residue. *S*-Acylation of proteins with fatty acids other than palmitate has been reported for a number of proteins (36–38). Furthermore, we have demonstrated that DHHC2 and DHHC3 have different acyl-CoA substrate specificities *in vitro*, but whether there is selective utilization of acyl-CoAs *in vivo* is unknown (20).

In this study, we establish the feasibility of directly identifying fatty acylated peptides using a C4-based LC-MS/MS method. Used in tandem with a C18 LC column, we obtained excellent sequence coverage of both hydrophobic and hydrophilic regions of DHHC3 and identified two peptides modified with palmitate. However, several issues must be addressed to improve recovery of *S*-acylated peptides. One limitation is the susceptibility of thioester linkages to hydrolysis during sample preparation (26), particularly under the conditions of prolonged trypsin digestion at pH 8 used for in-gel digests of proteins. The use of proteases that function at acidic pH may be helpful in this regard. It is also noteworthy that the two DHHC3 peptides that we recovered using direct detection were singly modified with palmitate, whereas using the acyl switch method, we recovered two tryptic peptides that were dually acylated. The elution profile of monolipidated peptides from the C4 reversed phase HPLC column suggested that dually palmitoylated peptides may have been too hydrophobic to be eluted with the acetonitrile gradient used in this method.[3] Accordingly, the use of different solvents for elution might improve recovery of the dually acylated peptides.

Although significant challenges remain for direct detection of *S*-acylated peptides, the method described here will be amenable for detection of peptides with *N*-linked fatty acids. The *N*-myristoylated peptide of $G\alpha_i$ was recovered reproducibly from tryptic digests of recombinant myristoylated $G\alpha_i$.[3] There is increasing interest in lysine-linked fatty acylation with the discovery that members of the sirtuin family are de-fatty acylases (39–41). Identifying the sites of lysine-linked fatty acids will be important in elucidating the biological consequences of this newly appreciated modification.

Author Contributions—C. D. G. and M. E. L. conceived and designed the study and wrote the paper. C. D. G. carried out all of the experiments with the exception of the mass spectrometry. S. Z. supervised collection of mass spectrometry data, contributed to experimental design, and wrote the section related to mass spectrometry under "Experimental Procedures."

Acknowledgments—We thank Martin Ian Malgapo for creating the FLAG-tagged DHHC3 baculovirus and for early experiments quantifying zinc on DHHC proteins. We thank Wendy Greentree for technical support and Wei Chen for enthusiastic and dedicated help in the design and execution of the mass spectrometry experiments. We thank Dr. Toshi Kawate and members of the Kawate laboratory, especially Kevin Michalski, for assistance with SEC analysis of purified DHHC3.

[3] C. D. Gottlieb, S. Zhang, and M. E. Linder, unpublished results.

References

1. Roth, A. F., Wan, J., Bailey, A. O., Sun, B., Kuchar, J. A., Green, W. N., Phinney, B. S., Yates, J. R., 3rd, and Davis, N. G. (2006) Global analysis of protein palmitoylation in yeast. *Cell* **125,** 1003–1013
2. Kang, R., Wan, J., Arstikaitis, P., Takahashi, H., Huang, K., Bailey, A. O., Thompson, J. X., Roth, A. F., Drisdel, R. C., Mastro, R., Green, W. N., Yates, J. R., 3rd, Davis, N. G., and El-Husseini, A. (2008) Neural palmitoyl-proteomics reveals dynamic synaptic palmitoylation. *Nature* **456,** 904–909
3. Martin, B. R., and Cravatt, B. F. (2009) Large-scale profiling of protein palmitoylation in mammalian cells. *Nat. Methods* **6,** 135–138
4. Sanders, S. S., Martin, D. D., Butland, S. L., Lavallée-Adam, M., Calzolari, D., Kay, C., Yates, J. R., 3rd, and Hayden, M. R. (2015) Curation of the mammalian palmitoylome indicates a pivotal role for palmitoylation in diseases and disorders of the nervous system and cancers. *PLoS Comput. Biol.* **11,** e1004405
5. Salaun, C., Greaves, J., and Chamberlain, L. H. (2010) The intracellular dynamic of protein palmitoylation. *J. Cell Biol.* **191,** 1229–1238
6. Blaskovic, S., Blanc, M., and van der Goot, F. G. (2013) What does *S*-palmitoylation do to membrane proteins? *FEBS J.* **280,** 2766–2774
7. Shipston, M. J. (2011) Ion channel regulation by protein palmitoylation. *J. Biol. Chem.* **286,** 8709–8716
8. Greaves, J., and Chamberlain, L. H. (2011) DHHC palmitoyl transferases: substrate interactions and (patho)physiology. *Trends Biochem. Sci.* **36,** 245–253
9. Young, F. B., Butland, S. L., Sanders, S. S., Sutton, L. M., and Hayden, M. R. (2012) Putting proteins in their place: palmitoylation in Huntington disease and other neuropsychiatric diseases. *Prog. Neurobiol.* **97,** 220–238
10. Yeste-Velasco, M., Linder, M. E., and Lu, Y. J. (2015) Protein *S*-palmitoylation and cancer. *Biochim. Biophys. Acta* **1856,** 107–120
11. Mitchell, D. A., Vasudevan, A., Linder, M. E., and Deschenes, R. J. (2006) Protein palmitoylation by a family of DHHC protein *S*-acyltransferases. *J. Lipid Res.* **47,** 1118–1127
12. Ohno, Y., Kashio, A., Ogata, R., Ishitomi, A., Yamazaki, Y., and Kihara, A. (2012) Analysis of substrate specificity of human DHHC protein acyl-

transferases using a yeast expression system. *Mol. Biol. Cell* **23,** 4543–4551
13. Yang, W., Di Vizio, D., Kirchner, M., Steen, H., and Freeman, M. R. (2010) Proteome scale characterization of human *S*-acylated proteins in lipid raft-enriched and non-raft membranes. *Mol. Cell. Proteomics* **9,** 54–70
14. Hemsley, P. A., and Grierson, C. S. (2011) The ankyrin repeats and DHHC *S*-acyl transferase domain of AKR1 act independently to regulate switching from vegetative to mating states in yeast. *PLoS One* **6,** e28799
15. Davda, D., El Azzouny, M. A., Tom, C. T., Hernandez, J. L., Majmudar, J. D., Kennedy, R. T., and Martin, B. R. (2013) Profiling targets of the irreversible palmitoylation inhibitor 2-bromopalmitate. *ACS Chem. Biol.* **8,** 1912–1917
16. Böhm, S., Frishman, D., and Mewes, H. W. (1997) Variations of the C2H2 zinc finger motif in yeast genome and classification of yeast zinc finger proteins. *Nucleic Acids Res.* **25,** 2464–2469
17. Mesilaty-Gross, S., Reich, A., Motro, B., and Wides, R. (1999) The *Drosphila* STAM gene homolog is in a tight gene cluster, and its expression correlates to that of the adjacent gene ial. *Gene* **231**
18. Putilina, T., Wong, P., and Gentleman, S. (1999) The DHHC domain: a new highly highly conserved cysteine-rich motif. *Mol. Cell Biochem.* **195,** 219–226
19. González Montoro, A., Quiroga, R., and Valdez Taubas, J. (2013) Zinc coordination by the DHHC cysteine-rich domain of the palmitoyltransferase Swf1. *Biochem. J.* **454,** 427–435
20. Jennings, B. C., and Linder, M. E. (2012) DHHC protein *S*-acyltransferases use similar ping-pong kinetic mechanisms but display different acyl-CoA specificities. *J. Biol. Chem.* **287,** 7236–7245
21. Jennings, B. C., Nadolski, M. J., Ling, Y., Baker, M. B., Harrison, M. L., Deschenes, R. J., and Linder, M. E. (2009) 2-Bromopalmitate and 2-(2-hydroxy-5-nitro-benzylidene)-benzo[b]thiophen-3-one inhibit DHHC-mediated palmitoylation *in vitro*. *J. Lipid Res.* **50,** 233–242
22. Lai, J., and Linder, M. E. (2013) Oligomerization of DHHC protein *S*-acyltransferases. *J. Biol. Chem.* **288,** 22862–22870
23. Yang, Y., Thannhauser, T. W., Li, L., and Zhang, S. (2007) Development of an integrated approach for evaluation of 2-D gel image analysis: impact of multiple proteins in single spots on comparative proteomics in conventional 2-D gel/MALDI workflow. *Electrophoresis* **28,** 2080–2094
24. Kawate, T., and Gouaux, E. (2006) Fluorescence-detection size-exclusion chromatography for precrystallization screening of integral membrane proteins. *Structure* **14,** 673–681
25. Simons, T. J. (1993) Measurement of free Zn^{2+} ion concentration with the fluorescent probe mag-fura-2 (furaptra). *J. Biochem. Biophys. Methods* **27,** 25–37
26. Ji, Y., Leymarie, N., Haeussler, D. J., Bachschmid, M. M., Costello, C. E., and Lin, C. (2013) Direct detection of *S*-palmitoylation by mass spectrometry. *Anal. Chem.* **85,** 11952–11959
27. Roth, A. F., Feng, Y., Chen, L., and Davis, N. G. (2002) The yeast DHHC cysteine-rich domain protein Akr1p is a palmitoyl transferase. *J. Cell Biol.* **159,** 23–28
28. Fang, C., Deng, L., Keller, C. A., Fukata, M., Fukata, Y., Chen, G., and Lüscher, B. (2006) GODZ-mediated palmitoylation of GABA(A) receptors is required for normal assembly and function of GABAergic inhibitory synapses. *J. Neurosci.* **26,** 12758–12768
29. Keller, C. A., Yuan, X., Panzanelli, P., Martin, M. L., Alldred, M., Sassoè-Pognetto, M., and Lüscher, B. (2004) The γ2 subunit of $GABA_A$ receptors is a substrate for palmitoylation by GODZ. *J. Neurosci.* **24,** 5881–5891
30. Cornell, N. W., and Crivaro, K. E. (1972) Stability constant for the zinc-dithiothreitol complex. *Anal. Biochem.* **47,** 203–208
31. Krezel, A., Latajka, R., Bujacz, G. D., and Bal, W. (2003) Coordination properties of tris(2-carboxyethyl)phosphine, a newly introduced thiol reductant, and its oxide. *Inorg. Chem.* **42,** 1994–2003
32. Mitchell, D. A., Mitchell, G., Ling, Y., Budde, C., and Deschenes, R. J. (2010) Mutational analysis of *Saccharomyces cerevisiae* Erf2 reveals a two-step reaction mechanism for protein palmitoylation by DHHC enzymes. *J. Biol. Chem.* **285,** 38104–38114
33. Pace, N. J., and Weerapana, E. (2014) Zinc-binding cysteines: diverse functions and structural motifs. *Biomolecules* **4,** 419–434
34. Hou, H., John Peter, A. T., Meiringer, C., Subramanian, K., and Ungermann, C. (2009) Analysis of DHHC acyltransferases implies overlapping substrate specificity and a two-step reaction mechanism. *Traffic* **10,** 1061–1073
35. Forrester, M. T., Hess, D. T., Thompson, J. W., Hultman, R., Moseley, M. A., Stamler, J. S., and Casey, P. J. (2011) Site-specific analysis of protein *S*-acylation by resin-assisted capture. *J. Lipid Res.* **52,** 393–398
36. Hallak, H., Muszbek, L., Laposata, M., Belmonte, E., Brass, L. F., and Manning, D. R. (1994) Covalent binding of arachidonate to G-protein a subunits of human platelets. *J. Biol. Chem.* **269,** 4713–4716
37. O'Brien, P. J., St Jules, R. S., Reddy, T. S., Bazan, N. G., and Zatz, M. (1987) Acylation of disc membrane rhodopsin may be nonenzymatic. *J. Biol. Chem.* **262,** 5210–5215
38. Wilson, J. P., Raghavan, A. S., Yang, Y. Y., Charron, G., and Hang, H. C. (2011) Proteomic analysis of fatty-acylated proteins in mammalian cells with chemical reporters reveals S-acylation of histone H3 variants. *Mol. Cell. Proteomics* 10.1074/mcp.M110.001198
39. Jiang, H., Khan, S., Wang, Y., Charron, G., He, B., Sebastian, C., Du, J., Kim, R., Ge, E., Mostoslavsky, R., Hang, H. C., Hao, Q., and Lin, H. (2013) SIRT6 regulates TNF-α secretion through hydrolysis of long-chain fatty acyl lysine. *Nature* **496,** 110–113
40. Feldman, J. L., Baeza, J., and Denu, J. M. (2013) Activation of the protein deacetylase SIRT6 by long-chain fatty acids and widespread deacylation by mammalian sirtuins. *J. Biol. Chem.* **288,** 31350–31356
41. Liu, Z., Yang, T., Li, X., Peng, T., Hang, H. C., and Li, X. D. (2015) Integrative chemical biology approaches for identification and characterization of "erasers" for fatty-acid-acylated lysine residues within proteins. *Angew. Chem. Int. Ed. Engl.* **54,** 1149–1152